Molecular Therapy
Nucleic Acids
Original Article

TGF-β1-triggered BMI1 and SMAD2 cooperatively regulate miR-191 to modulate bone formation

Xiao-Fei Zhang,[2,6] Zi-Xuan Wang,[3,6] Bo-Wen Zhang,[3] Kun-Peng Huang,[3] Tian-Xing Ren,[3] Ting Wang,[1] Xing Cheng,[4] Ping Hu,[3] Wei-Hua Xu,[5] Jin Li,[5] Jin-Xiang Zhang,[3] and Hui Wang[1]

[1]Department of Medical Genetics, School of Basic Medicine, Tongji Medical College, Huazhong University of Science and Technology, Wuhan, Hubei, 430030, China; [2]Center for Translational Medicine, Union Hospital, Tongji Medical College, Huazhong University of Science and Technology, Wuhan, Hubei, 430000, China; [3]Department of Emergency Surgery, Union Hospital, Tongji Medical College, Huazhong University of Science and Technology, Wuhan, Hubei, 430000, China; [4]Health Care Management Center, Union Hospital, Tongji Medical College, Huazhong University of Science and Technology, Wuhan, Hubei, 430000, China; [5]Department of Orthopedics, Union Hospital, Tongji Medical College, Huazhong University of Science and Technology, Wuhan, Hubei, 430000, China

Transforming growth factor β 1 (TGF-β1), as the most abundant signaling molecule in bone matrix, is essential for bone homeostasis. However, the signaling transduction of TGF-β1 in the bone-forming microenvironment remains unknown. Here, we showed that microRNA-191 (miR-191) was downregulated during osteogenesis and further decreased by osteo-favoring TGF-β1 in bone marrow mesenchymal stem cells (BMSCs). MiR-191 was lower in bone tissues from children than in those from middle-aged individuals and it was negatively correlated with collagen type I alpha 1 chain (*COL1A1*). MiR-191 depletion significantly increased osteogenesis and bone formation *in vivo*. Hydrogels embedded with miR-191-low BMSCs displayed a powerful bone repair effect. Mechanistically, transcription factors BMI1 and SMAD2 coordinately controlled miR-191 level. In detail, BMI1 and pSMAD2 were both upregulated by TGF-β1 under osteogenic condition. SMAD2 activated miR-191 transcription, while BMI1 competed with SMAD2 for binding to miR-191 promoter region, thus disturbing the activation of SMAD2 on miR-191 and reducing miR-191 level. Altogether, our findings reveal that miR-191 regulated by TGF-β1-induced BMI1 and SMAD2 negatively modulated bone formation and regeneration, and inhibition of miR-191 might be therapeutically useful to enhance bone repair in clinic.

INTRODUCTION

Bone formation by osteoblasts is a crucial process after bone injuries.[1] Bone marrow-derived mesenchymal stem cells (BMSCs) are the sources of osteoprogenitor cells, which can differentiate into osteoblasts and induce bone formation.[2] During bone healing, BMSCs can be recruited by various cytokines and chemokines to injured sites, where they proliferate, differentiate, modulate cell-cell communications via paracrine modes, and consequently lead to bone regeneration and fracture healing, which makes them ideal for bone tissue engineering.[3–6] Thus, in-depth understanding of molecular mechanisms governing the behaviors of BMSCs and developing novel strategies to promote bone formation and regeneration are necessary.

Transforming growth factor β 1 (TGF-β1) is the most concentrated and important microenvironment signal molecule during bone formation and remodeling and it is highly activated during bone injury.[7–9] However, the effect of TGF-β1 on BMSC osteogenesis and bone formation is bidirectional and depends on various factors, including its dosage and cellular context.[8,10–14] Thus, exploring the key downstream targets of specific TGF-β1 responses may enable the discovery of new therapeutic options for bone-related diseases. SMAD proteins are the major intracellular transmitters of TGF-β signaling. They form complexes that can bind to Smad binding elements in the promoter region of target genes, thus activating TGF-β responses.[14,15] In response to certain microenviromental cues, SMADs can also recruit other transcriptional factors or co-regulators to direct the expression of specific downstream genes to provoke certain TGF-β responses.[16] Polycomb protein bmi-1 (BMI1, also known as PCGF4) is a major component of Polycomb-repressive complex 1 (PRC1), which acts as an essential epigenetic corepressor of target genes.[17] BMI1 could promote osteogenesis of BMSCs and protect against osteoporosis in mice.[18–22] Previous study reported PCGF5, another PRC1 protein, could epigenetically regulate SMAD2/TGF-β signaling to enhance neural differentiation[23]; however, there is currently no evidence regarding the potential interplay between BMI1 and TGF-β/SMADs signaling. Based on these grounds, finding the key targets of certain TGF-β responses and exploring their transcriptional regulatory mode by SMADs and/or other transcription regulators under specific microenvironment will enrich the signal transduction mechanism of TGF-β and provide a new strategy for bone healing.

MicroRNA-191 (miR-191) plays a critical role in various tumors and diseases including ischemia-induced tissue injury by regulating

Received 25 June 2023; accepted 4 March 2024;
https://doi.org/10.1016/j.omtn.2024.102164.

[6]These authors contributed equally

Correspondence: Hui Wang, PhD, Department of Medical Genetics, School of Basic Medicine, Tongji Medical College, Huazhong University of Science and Technology, Wuhan 430000, China.
E-mail: wanghuipitt@hust.edu.cn

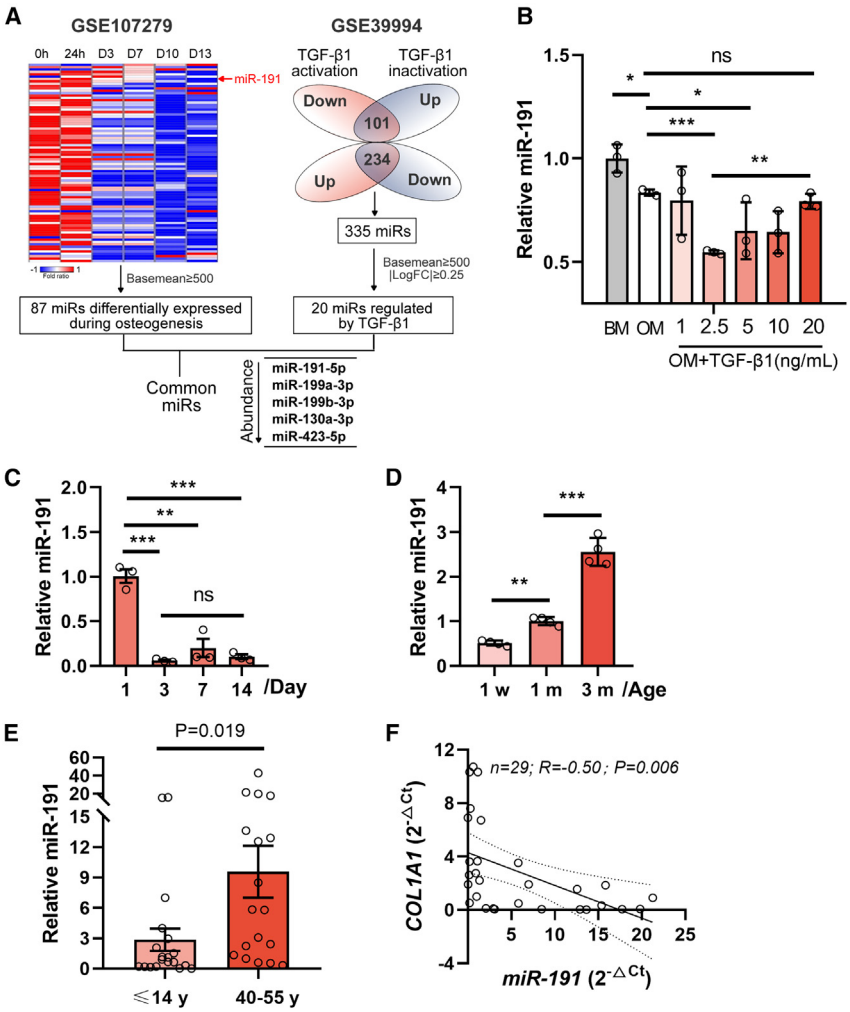

Figure 1. MiR-191 was regulated by TGF-β1 under osteogenic condition

(A) The re-analysis of GEO: GSE107279 and GEO: GSE39994 to screen miRNAs regulated by TGF-β1 and osteogenic induction. (B–D) The levels of miR-191 in BMSCs treated with basal media (BM, complete media), osteogenic media (OM), and OM supplemented with TGF-β1 (OM+TGF-β1) at the indicated concentrations (B), in BMSCs cultured in OM at the indicated time points (C), and in bone tissues collected from mice at 1 week (w), 1 month (m), or 3 months of age (D). The data are presented as the mean ± SDs. (E) The levels of miR-191 in bone specimens from children (≤14 years) and middle-aged individuals (40–55 years). n = 19 for the children's group, n = 18 for the middle-aged group, respectively. All data are presented as the mean ± SEMs. (F) The correlation analysis of miR-191 with *COL1A1* in human bone tissues. The significance is indicated as *p < 0.05, **p < 0.01, ***p < 0.001. ns = no significance.

different cellular processes.[24,25] The function of miR-191 varies according to the specific cell type or the context.[24] Cellular stresses such as hypoxia,[25] radiation,[26] or chemotherapeutic drugs[27] can influence the expression of miR-191. Additionally, the level of miR-191 was associated with tissue development and has been found to be dysregulated during human and mouse embryonic development.[28,29] Moreover, miR-191 has been observed to gradually decline during the osteogenesis of BMSCs,[30] suggesting its involvement in the regulation of cellular function of BMSCs and subsequent bone formation. However, the precise function and mechanism of miR-191 require further elucidation.

In this study, we found that TGF-β1 downregulated miR-191 under osteogenic conditions. Mice lacking miR-191 exhibited strong bone formation with an increase of osteoblast number. Hydrogels embedded with miR-191-low BMSCs induced bone repair *in vivo*. *In vitro* study demonstrated that inhibition of miR-191 promoted osteogenesis, increased the secretion of monocyte chemoattractant protein-1 (MCP-1, also known as CCL2), and enhanced the migration of BMSCs. We also discovered a novel competitive binding mode of transcription factors BMI1 and SMAD2, which cooperatively regulate the transcription of miR-191. Collectively, our research highlights miR-191 as a key downstream target of TGF-β1 signaling in bone homeostasis and suggests that suppression of miR-191 may be therapeutically effective for bone regeneration.

RESULTS

MiR-191 participates in TGF-β1-regulated osteogenesis of BMSCs

The impact of TGF-β1 on osteogenesis of BMSCs is bidirectional and depends on its dosage and cellular context.[8,10,31] Given that the appropriate dose of TGF-β1 *in vivo* stimulates bone development and improves bone cell function,[32–35] we first investigated the effect of different TGF-β1 concentrations on osteogenesis of BMSCs in order to find the optimal dose of TGF-β1 to enhance osteogenesis. We found that 2.5 ng/mL TGF-β1 induced the osteogenic proteins in BMSCs, while 10 or 20 ng/mL TGF-β1 decreased them (Figure S1A), which was partially consistent with a previous report in which 1 ng/mL TGF-β1 was osteo-promotive, whereas 10 ng/mL TGF-β1 or above concentrations were osteo-inhibitory under osteogenic conditions.[10] To screen the candidate microRNAs regulated by both osteogenic induction and TGF-β1, we re-analyzed GEO: GSE107279 (differentially expressed microRNAs during osteogenesis of human BMSCs[30]) and GEO: GSE39994 (differentially expressed microRNAs in embryonic stem cells treated with TGF/Smads activator or inhibitor[36]), and found five common microRNAs including miR-191-5p, miR-199a-3p, miR-199b-3p, miR-130a-3p, and miR-423-5p (Figure 1A; Table S1). The results of quantitative PCR (qPCR) confirmed that osteogenic induction downregulated miR-191-5p and miR-423-5p, and

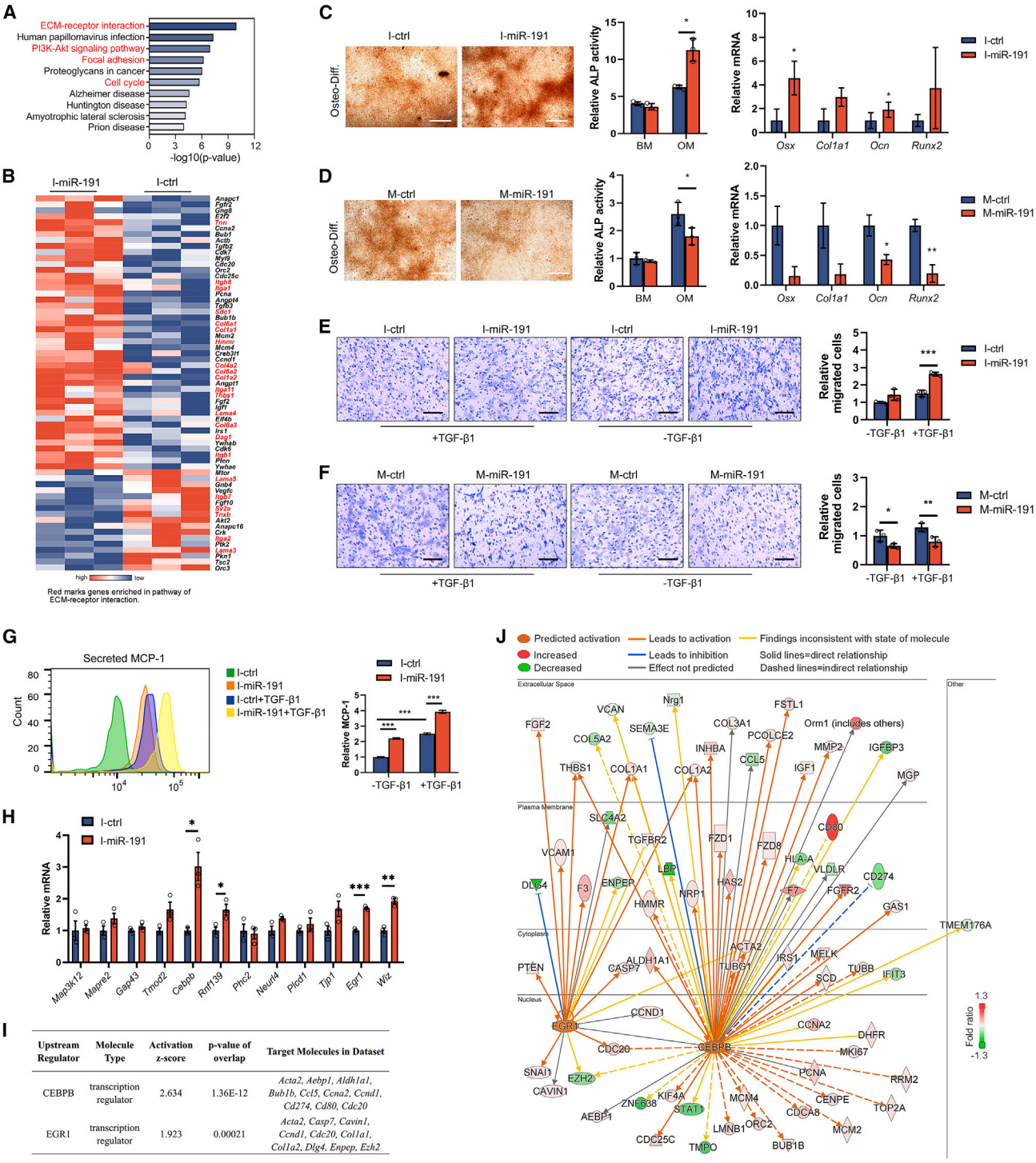

Upstream Regulator	Molecule Type	Activation z-score	p-value of overlap	Target Molecules in Dataset
CEBPB	transcription regulator	2.634	1.36E-12	*Acta2, Aebp1, Aldh1a1, Bub1b, Ccl5, Ccna2, Ccnd1, Cd274, Cd80, Cdc20*
EGR1	transcription regulator	1.923	0.00021	*Acta2, Casp7, Cavin1, Ccnd1, Cdc20, Col1a1, Col1a2, Dlg4, Enpep, Ezh2*

Figure 2. Knockdown of miR-191 increases BMSC osteogenesis

(A) BMSCs transfected with inhibitor control oligos (l-ctrl) or inhibitor-miR-191 oligos (l-miR-191) and cultured in osteogenic media for 48 h were subjected to RNA sequencing. KEGG pathway enrichment of the differentially expressed genes (DEGs, $p < 0.05$) was analyzed by DAVID (https://david.ncifcrf.gov/). (B) Heatmap representation of dysregulated genes enriched in pathways including ECM-receptor interaction, PI3K-Akt signaling pathway, focal adhesion, and cell cycle. (C and D) Representative images of alkaline phosphatase staining (day 14 of culture), ALP activities (day 5 of culture), and the mRNA levels of the indicated marker genes (day 3 of culture) in BMSCs transfected with l-miR-191/l-ctrl (C) or mimic control oligos (M-ctrl)/mimic-miR-191 oligos (M-miR-191) (D) and cultured in osteogenic induction media. BM (basal

(legend continued on next page)

upregulated miR-199a-3p, but had no effect on miR-130a-3p and miR-199b-3p in BMSCs; TGF-β1 had variable effects on the levels of all five microRNAs. Notably, the expression of miR-191-5p was obviously reduced by 2.5 ng/mL TGF-β1, and it recovered to pre-treated level by 20 ng/mL TGF-β1 compared with osteogenic media group (Figures 1B and S1B). Given the close correlation of its expression pattern and the effect of TGF-β1 on osteogenesis, miR-191-5p was chosen for further study. We further showed that miR-191 was reduced markedly at day 3 and maintained at low levels at day 7 and day 14 of osteogenic culture of osteogenic media, indicating a key role of miR-191 at the early stage of osteogenesis (Figure 1C). We also observed a gradual increase in the level of miR-191 in mouse bone tissues as the age of the mice increased from 1 week, 1 month old to 3 months old (Figure 1D), suggesting miR-191 may play a role in bone development. Moreover, we analyzed the levels of miR-191 in human bone specimens, including 18 samples from middle-aged adults (40–55 years) and 19 samples from children (0–14 years), with the clinical information provided in Table S2. We found that miR-191 was significantly lower in bone tissues from children compared with those from middle-aged individuals (Figure 1E). Type I collagen is one of the most important extracellular matrix components of bone tissues, and its encoding gene *COL1A1* is a key downstream effector of TGF-β1 signaling in various cells.[37–41] In combination with the differential expression of miR-191 during bone development observed above, we analyzed the relationship between miR-191 and *COL1A1* in human specimens. The results indicated that miR-191 was inversely related to *COL1A1* ($R = -0.5$, $p = 0.006$) in human bone tissues (Figure 1F). The above data strongly suggest an involvement of miR-191 in bone development and a close correlation between miR-191 and the function of TGF-β1 in osteogenesis of BMSCs.

Inhibition of miR-191 promotes osteogenesis of BMSCs *in vitro*

Since miR-191 was found to be decreased during osteogenesis of BMSCs, we explored the impact of miR-191 on BMSCs by utilizing mimics and inhibitors of miR-191 (Figure S2). RNA sequencing revealed that differentially expressed genes (DEGs) in BMSCs transfected with inhibitor control or inhibitor of miR-191 were mainly enriched in KEGG pathways of extracellular matrix (ECM)-receptor interaction, PI3K-Akt signaling pathway, focal adhesion, and cell cycle, all of which are critical for cell survival and differentiation of BMSCs (Figure 2A). The DEGs within those pathways were depicted in a heatmap, with more than 70% of them increased in the inhibitor-miR-191 transfected group, especially collagen genes, suggesting a regulation of miR-191 on ECM production of BMSCs following osteogenic induction (Figure 2B). The results of cell staining assays and alkaline phosphatase (ALP) activity assays confirmed that inhibition of miR-191 promoted mineral deposition, whereas overexpression of miR-191 decreased mineral deposition (Figures 2C and 2D). *Osx* and *Runx2* are the key osteogenic transcription factors that regulate the differentiation of BMSCs into osteoblasts. *Ocn* and *Col1a1* are specific osteoblast marker genes. qPCR results indicated that inhibition of miR-191 increased the expression of *Osx, Col1a1*, *Ocn*, and *Runx2*, while upregulation of miR-191 reduced their expression (Figures 2C and 2D). Moreover, inhibition of miR-191 further increased TGF-β1-induced migratory activity of BMSCs, while miR-191 mimic decreased cell migration (Figures 2E and 2F). In addition, downregulation of miR-191 raised TGF-β1-induced MCP-1 secretion (Figure 2G). These findings showed that miR-191 was a critical regulator of BMSC behaviors.

Then we screened for the targets of miR-191 using the ENCORI database (https://rnasysu.com/encori/), which incorporates predictive information from databases such as Pictar and TargetScan. We found 14 common targets of miR-191 across the PicTar, TargetScan, and miRanda databases, as shown in Table S3. We checked the expression of those molecules in our sequencing results (the DEGs between miR-191 inhibitor group and inhibitor control group [DEGs, $p < 0.05$, $|\log FC| > 0.1$]). However, the p values of these molecules are greater than 0.05, thus, we detected their levels in BMSCs transfected with miR-191 inhibitor or inhibitor control and cultured in osteogenic media for 72 h. The results indicated that Cebpb, Rnf139, Egr1, and Wiz were significantly upregulated in the miR-191 inhibitor group compared with the control group (Figure 2H), suggesting that these molecules might be the key targets of miR-191 during osteogenesis.

QIAGEN ingenuity pathway analysis (IPA) upstream regulator analysis tool was employed to obtain all the predicted upstream regulators of the DEGs from RNA sequencing data (Table S4). Through this analysis, we successfully identified two molecules, CEBPB and EGR1, that showed overlap between the upstream regulators and the targets of miR-191. Consistent with our expectations, the signals associated with the two molecules were found to be activated in IPA, with *Z* score of 2.6 and 1.9, respectively (Figure 2I). The regulatory networks of EGR1 and CEBPB and their downstream molecules are shown as Figure 2J. The above data suggested that Cebpb and Egr1, acting as the key targets of miR-191, could play a primary role in miR-191-regulated osteogenesis of BMSCs.

Additionally, the upstream regulator analysis by IPA also revealed that TGF-β1 signaling was activated in miR-191 inhibitor group (*Z* score = 3.094, Figures S3A and S3B), implying that inhibition of

media), OM (osteogenic media). Scale bar, 250 μm. The data are presented as the mean ± SDs. (E and F) Representative images of Transwell-migrated BMSCs transfected with I-ctrl/I-miR-191 (E) or M-ctrl/M-miR-191 (F) and exposed to complete media or complete media with TGF-β1 of 2.5 ng/mL for 48 h. Scale bar, 200 μm. The data are presented as the mean ± SDs. (G) MCP-1 levels in the supernatants of BMSCs following transfection with the indicated oligos and exposed to complete media or complete media with TGF-β1 of 2.5 ng/mL) for 48 h, as determined by a cytometric bead array system. The data are presented as the mean ± SDs. (H) The levels of the predicted targets of miR-191 in BMSCs transfected with the indicated oligos. The data are presented as the mean ± SEMs. (I) The common molecules between QIAGEN ingenuity pathway analysis predicted upstream regulators and the verified miR-191 targets, and the DEPs regulated by them. (J) The regulatory networks of EGR1 and CEBPB and their downstream molecules generated by IPA. The significance is shown as *$p < 0.05$, **$p < 0.01$, and ***$p < 0.001$.

miR-191 enhanced TGF-β1 signaling, leading to increased expression of TGF-β1 downstream effectors. Given that miR-191 was decreased by TGF-β1 at 2.5 ng/mL (Figure 1B), these data further indicated that the decrease in miR-191 levels is an important event in response to the osteo-favoring TGF-β1.

MiR-191 deficiency is favorable for bone formation and repair

To investigate the effect of miR-191 loss on bone formation, we first assessed bone parameters in miR-191-deficient mice. Microcomputed tomography (μCT) on the long bones revealed increased trabecular bone formation in the endocortical compartment in miR-191$^{-/-}$ mice (Figures 3A and 3B). When compared with wild-type (WT, miR-191$^{+/+}$) mice, trabecular bone volume (BV/TV), bone surface density (BS/TV), and number (Tb.N) were increased, while trabecular separation (Tb.Sp) was reduced in the femora of miR-191$^{-/-}$ mice (Figure 3C). There were no noticeable variations in trabecular thickness (Tb.Th) and pattern factors (Tb.Pf) (Figure 3C). The cortical thickness (Ct.Th) was greater in miR-191$^{-/-}$ mice than in WT (miR-191$^{+/+}$) littermates (Figure 3D). The results of calcein double labeling showed that miR-191-deleted mice had notably higher mineralization apposition rate (MAR) and bone formation rate (BFR) in the cortical bones and cancellous bones proximal to the growth plate of the distal femurs than WT mice (Figures 3E–3G).

Femoral sections demonstrated an elevated number of osteoblasts ($p = 0.02$) and a comparable number of osteoclasts (no significance, $p = 0.24$) on the trabecular bone surfaces (Figures 3H and 3I) of miR-191$^{-/-}$ mice compared with WT mice. Consistently, the serum levels of procollagen type I N-propeptide, which is a marker of bone formation, raised significantly in miR-191-deleted mice than in WT mice, whereas osteoblast activity marker of C-terminal telopeptide of type I collagen (CTX-I) was comparable between miR-191$^{-/-}$ mice and WT mice (Figure 3J). Furthermore, collagen I was increased in osteoblasts and lining cells surrounding trabecular bones in miR-191$^{-/-}$ mice (Figure 3K). In addition, the deletion of miR-191 caused a significant increase in calcium deposition, ALP activities, and osteogenesis-related genes (Figure 3L). These findings collectively demonstrated the dominant role of miR-191 deficiency in bone formation.

BMSCs are crucial participants in bone fracture healing. TGF-β1 is highly activated during bone repair. We have found that miR-191 was closely related to TGF-β1-regulated osteogenesis of BMSCs. Thus, we further explored the role of miR-191 on BMSC-mediated bone repair in the presence of TGF-β1. We generated a transcortical defect hole with a 0.8-mm diameter of drill through a cortex of the mouse tibia (Figure S4). In this model, bone regeneration occurs exclusively through intramembranous ossification, which greatly depends on BMSC osteogenesis under the TGF-β1 stimulation at the damaged site, without intervening cartilage intermediates.[42,43] μCT was performed to assess the regenerated bone in the tibia defect at postsurgery days 3 and 7 (PSD3, PSD7). The views of three-dimensional (3D) reconstruction showed that miR-191 knockout resulted in more mineral deposition compared with WT mice (Figure 3M). There was a significant increase in bone volume, surface density and trabecular number of newly formed bone in miR-191$^{-/-}$ mice (Figure 3N). Trabecular separation was significantly decreased in miR-191$^{-/-}$ mice (Figure 3N). Trabecular thickness and trabecular pattern factor were not significantly altered (Figure 3N). All the above data illustrated that miR-191 greatly impacted osteogenesis of BMSCs during bone formation and healing.

Localized inhibition of miR-191 of BMSCs effectively enhances osteogenic differentiation and bone repair *in vivo*

We have confirmed the essential function of miR-191 in osteogenesis of BMSCs. To further identify the potential therapeutic effect of miR-191-regulated BMSCs on bone regeneration, we constructed a 3D culture system with GelMA hydrogels embedded with BMSCs overexpressing or down-expressing miR-191. The flowchart is shown in Figure 4A. Photocrosslinkable GelMA was easy to shape within minutes, and GelMA hydrogels were transparent (Figure 4B). BMSCs displayed a round morphology in GelMA hydrogels, and more than 90% of cells survived after 48 h of 3D culture, as evidenced by the live/dead assay (Figure 4C), indicating the good biocompatibility of GelMA. The GelMA scaffold was highly porous with an average pore diameter of 48.72 ± 12.28 μm (Figure 4D), which was suitable for cell proliferation and communication. Notably, BMSCs grew and formed spheres (red arrow) in GelMA hydrogels (Figure 4D). Alizarin Red staining analysis showed that the mineral deposition was remarkably lower in 3D cultured BMSCs overexpressing miR-191, whereas suppressing miR-191 led to a marked increase in mineralization (Figures 4E and G). Consistently, the levels of *Osx*, *Col1a1*, and *Runx2* were prominently activated in the miR-191 downregulated group but reduced in the miR-191 overexpressing group (Figures 4F and H).

Then, a tibia injury model was established. The defective holes in tibias were injected with GelMA/BMSC mixture (5 μL) and irradiated by a long wavelength UV lamp for 5 min. Seven days after surgery, μCt scanning showed that more bone-like tissues were formed in mice implanted with GelMA hydrogels loaded with miR-191 downregulated BMSCs (Figure 4I). The reconstructed 3D views of injured tibia revealed that miR-191 inhibitor induced more mineralization compared with the control group (Figure 4I). μCt analysis further revealed that GelMA hydrogel-treated tibias showed elevated BV/TV, BS/TV, and Tb.N. BMSC addition further increased bone formation, as indicated by the increased BV/TV, BS/TV, and Tb.N, and the decreased Tb.Pf in comparison with the GelMA hyrdrogel-treated group. Among the four groups, hydrogels embedded with miR-191 knockdown BMSCs showed the highest levels of BV/TV, BS/TV, Tb.N, and Tb.Th as well as the lowest levels of BS/BV and Tb.Pf (Figure 4J). Taken together, our results illustrated that miR-191 downregulation in BMSCs enhanced osteogenesis and bone repair *in vitro* and *in vivo,* and suppression of miR-191 could be a potential strategy for the treatment of bone injuries.

SMAD2 induces miR-191 transcription

Next, we investigated the upstream transcriptional regulatory mechanism of miR-191 in response to TGF-β1 under osteogenic conditions. Since SMAD2/3/4 proteins are well-known key intracellular mediators

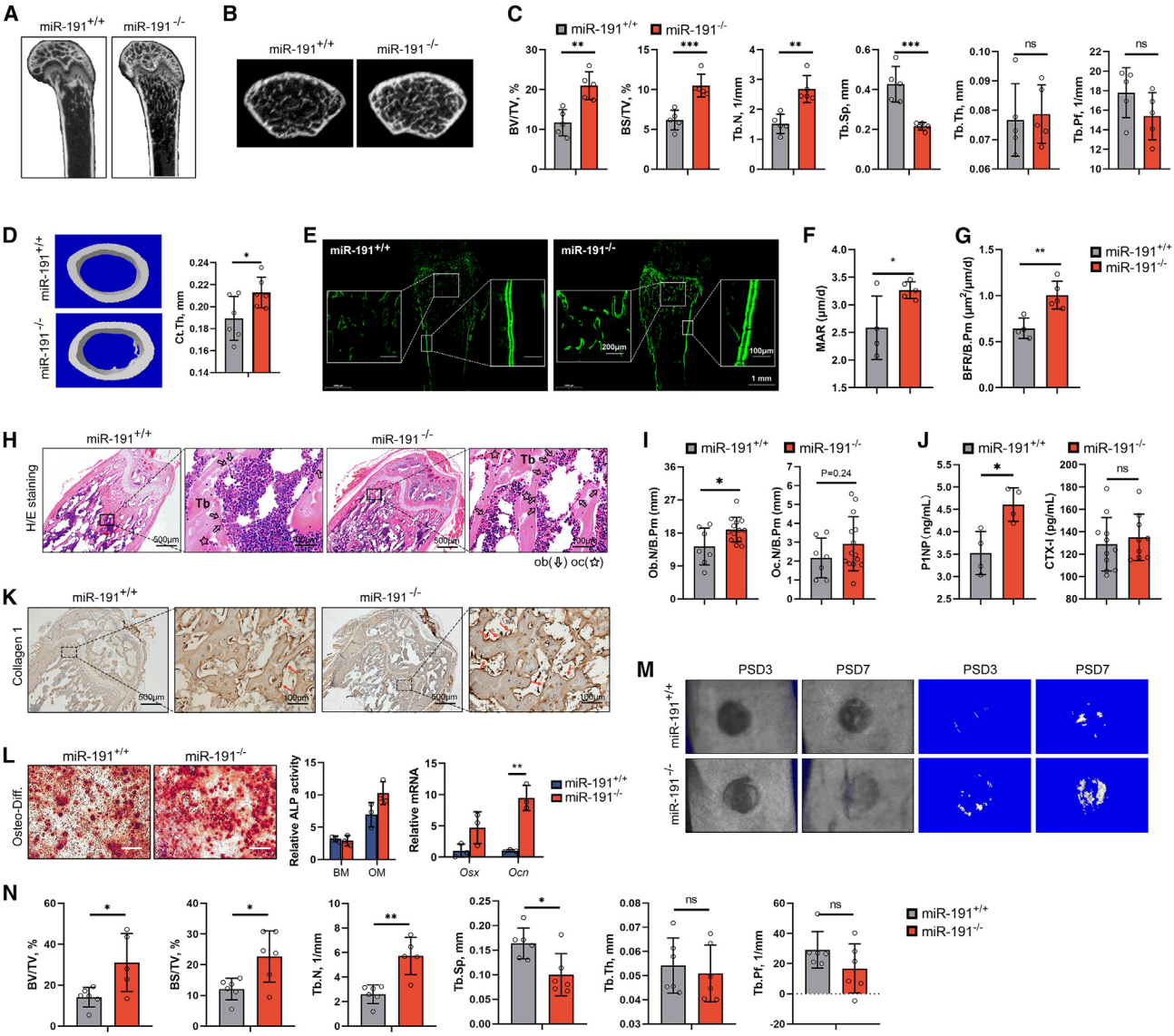

Figure 3. Deletion of miR-191 promotes bone formation

(A and B) Representative images of μCT analysis of the endocortical compartment of femurs collected from 8-week-old miR-191$^{+/+}$ and miR-191$^{-/-}$ mice. (C) Quantitative assessments of BV/TV, BS/TV, Tb.N, Tb.Sp, Tb.Th, and Tb.Pf of femurs from 8-week-old miR-191$^{+/+}$ and miR-191$^{-/-}$ mice. (D) Representative μCT images of cortical bone from 8-week-old miR-191$^{+/+}$ and miR-191$^{-/-}$ mice, and the thickness (Ct.Th.) was analyzed. (E) Representative calcein dual labeling images of the metaphyseal cancellous bones and the diaphyseal cortical bones (right) of 6-week-old miR-191$^{+/+}$ and miR-191$^{-/-}$ mice. The scale bars are shown as indicated. (F and G) Quantitative analysis of the mineralization apposition rate (MAR) (F) and bone formation rate (BFR) per bone perimeter (B.Pm) (G). (H) Representative H&E staining images of distal femurs from 8-week-old miR-191$^{+/+}$ and miR-191$^{-/-}$ mice. Arrows represent osteoblasts, and stars indicate osteoclasts. The scale bars are shown as indicated. (I) Osteoblast number (ob.N/B.Pm) and osteoclast number (oc.N/B.Pm) in miR-191$^{+/+}$ and miR-191$^{-/-}$ mice at 8 weeks of age. (J) ELISA of serum P1NP and CTX-I in 8-week-old miR-191$^{+/+}$ and miR-191$^{-/-}$ mice. (K) Representative immunostaining of collagen 1 in distal femurs from 8-week-old miR-191$^{+/+}$ and miR-191$^{-/-}$ mice. The scale bars are shown as indicated. (L) Representative Alizarin Red staining images, ALP activities, and the levels of *Osx* and *Ocn* of miR-191$^{+/+}$ and miR-191$^{-/-}$ BMSCs cultured in osteogenic media. Scale bar, 250 μm. (M and N) 12-week-old miR-191$^{+/+}$ and miR-191$^{-/-}$ mice were subjected to tibia monocortical bone defect surgery. Representative images of μCT of tibias at postsurgery days (PSDs) 3 and 7 (M) and quantification of the indicated characteristics of injured tibias (N). The significance is shown as *p < 0.05, **p < 0.01, and ***p < 0.001. ns = no significance. All data are presented as the mean values ± SDs.

of TGF-β1 signaling, we speculate that SMADs might regulate the transcription of miR-191. The results from the luciferase assay showed that SMAD2 overexpression facilitated the reporter activity of miR-191 5′UTR, but overexpression of SMAD3 or SMAD4 had no significant effect (Figures 5A and S5), implying that miR-191 was specifically activated by SMAD2. In addition, SMAD2 increased the 5′UTR activity

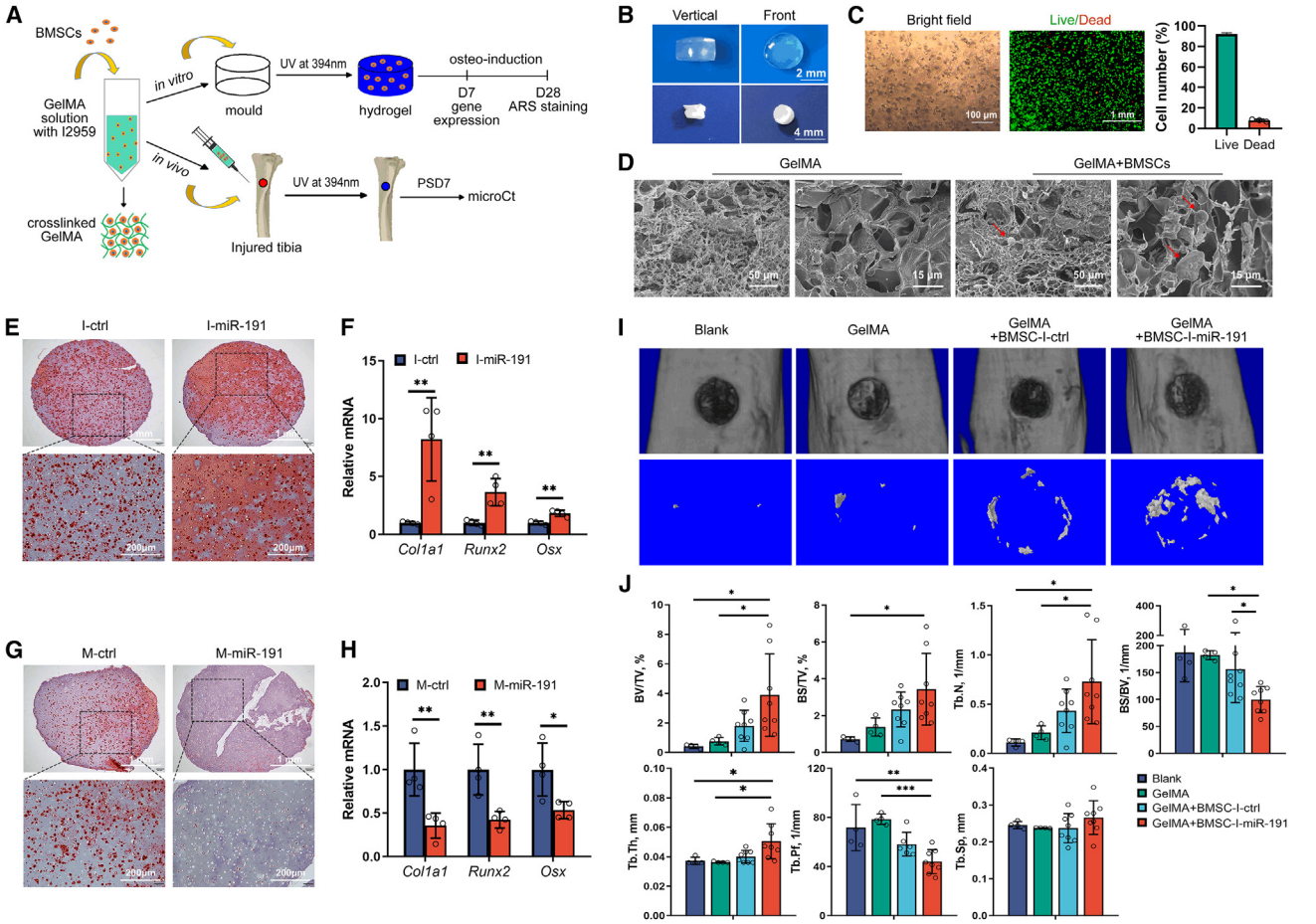

Figure 4. Inhibition of miR-191 effectively enhances osteogenic differentiation and bone formation

(A) Work flowchart of the experiments *in vitro* and *in vivo*. (B) Images of GelMA hydrogels before and after freeze-drying. The scale bars are shown as indicated. (C) Representative images of bright-field microscopy and live/dead assays of BMSCs embedded in GelMA hydrogels, as well as quantification of live cell numbers. The scale bars represent 100 μm on the left and 1 mm on the right, respectively. (D) Representative images of freeze-dried GelMA hydrogels embedded with or without BMSCs observed by scanning electron microscopy (SEM). The scale bars represent 50 μm and 15 μm, as indicated. The red arrow points to cells in hydrogels. (E–H) BMSCs were transfected with the indicated oligos, embedded in hydrogels, and cultured in osteogenic induction media. After 7 days, the osteogenic marker genes *Col1a1*, *Runx2*, and *Ocn* were detected (F and H), and after 28 days, cells were stained with Alizarin Red (E and G). The scale bars are shown as indicated. (I) Tibia monocortical bone defect surgery was performed on WT mice at 12 weeks of age. The defects were not treated (Blank group), or treated with GelMA hydrogels (GelMA group), GelMA hydrogels embedded with BMSCs transfected with I-ctrl oligos (GelMA+BMSC-I-ctrl group), or GelMA hydrogels embedded with BMSCs transfected with I-miR-191 oligos (GelMA+BMSC-I-miR-191 group). Representative images of μCT of tibias at postsurgery day 7. (J) Quantitative measurements of the indicated parameters of injured tibias. The significance is shown as $^{*}p < 0.05$, $^{**}p < 0.01$, and $^{***}p < 0.001$. All data are presented as the mean ± SDs.

of miR-191 in a dose-dependent manner (Figure 5B). Accordingly, up-regulation of SMAD2 induced miR-191 expression (Figure 5C). By employing animal TFDB (https://guolab.wchscu.cn/AnimalTFDB4/#/), we found seven binding sites of SMAD2 within 2,000 base pairs (bp) upstream sequence from the transcription start site of miR-191 gene with the consensus binding element CAGAC (Figure 5D). Further chromatin immunoprecipitation (ChIP) assays indicated that the sequence products containing the binding sites of S2/S3 (−644 to −656 bp and −718 to −725 bp) and S5 (−1,039 to −1,050 bp) were highly enriched by SMAD2 antibody precipitation (Figure 5E). Moreover, we observed an increase of phosphorylated SMAD2 in BMSCs cultured in osteogenic media supplemented with TGF-β1 (2.5 ng/mL and 20 ng/mL) compared with those in BMSCs cultured in basal media (Figure 5F), while overexpression of *Smad2* suppressed the levels of osteogenic marker genes (Figure S6), indicating that both the activation status and the abundance of SMAD2 were important for its effect on the osteogenesis of BMSCs. Taken together, these data indicated that TGF-β1/SMAD2 signaling induced miR-191 expression, but it was contrary to the reduction of miR-191 upon 2.5 ng/mL TGF-β1 stimulation under osteogenic conditions, as shown in Figure 1B, implying that TGF-β1 might modulate other transcription factors to inhibit the activation of SMAD2 on miR-191.

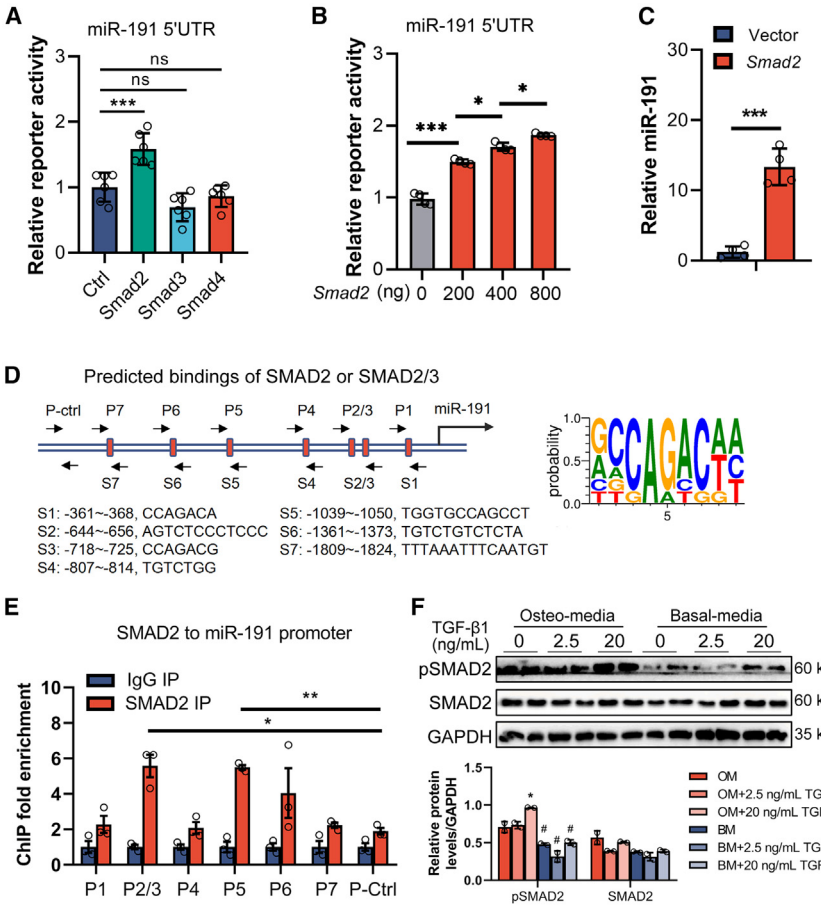

Figure 5. SMAD2 transcriptionally activates miR-191

(A and B) Luciferase analysis of reporter activity of miR-191 5′UTR in HEK293T cells transfected with plasmids overexpressing *Smad2*, *Smad3*, or *Smad4* (A), and in HEK293T cells transfected with *Smad2* at the indicated concentrations (B). The data are presented as the mean ± SDs. (C) miR-191 levels quantified by RT-PCR in HEK293T cells transfected with 1 μg of pHAGE-*Smad2*. The data are presented as the mean ± SDs. (D) The predicted sequence and possibility analysis of the SMAD2 binding sequence at the miR-191 promoter. "P" represents the primer position relative to the seven binding sites. (E) ChIP assays of SMAD2 on the miR-191 promoter in HEK293T cells. The data are presented as the mean ± SEMs. (F) Western blotting analysis of phosphorylated SMAD2 and SMAD2 levels in BMSCs cultured under the indicated conditions. *p < 0.05 vs. OM group; #p < 0.05 vs. the same concentration of TGF-β1 under OM conditions. The data are presented as the mean ± SEMs. The significance is shown as *p < 0.05, **p < 0.01, and ***p < 0.001. ns = no significance.

TGF-β1-triggered BMI1 disrupts miR-191 activation through competitively inhibiting the binding of SMAD2 to the promoter of miR-191

To further investigate the upstream transcription factors downregulating miR-191 upon TGF-β1 stimuli, we performed RNA sequencing to find the DEGs in BMSCs cultured in osteogenic media (OM) or OM with an additional 2.5 ng/mL TGF-β1 (Figure 6A). We compared the DEGs with all transcription factors in the TRRUST database (https://www.grnpedia.org/trrust/downloadnetwork.php) and screened the common genes. Among them, the transcription regulator *Bmi1* was increased most significantly in response to TGF-β1 ($p \leq 0.005$; Figure 6B). The upregulation of BMI1 was validated in BMSCs cultured in OM with 2.5 ng/mL TGF-β1 (Figure 6C). Moreover, we observed a negative correlation of BMI1 with miR-191 in human bone tissues, which further addressed the clinical significance of BMI1 and miR-191 in human bone formation (Figure 6D). Consistent with previous reports,[18,21,44] BMI1 overexpression enhanced the expression of osteogenic marker genes, including *Col1a1*, *Ocn*, and *Osx* in BMSCs, and vice versa (Figures S7A and S7B). Furthermore, we observed that suppression of *Bmi1* impaired the ability of TGF-β1 to promote osteogenesis (Figure S7C). All the above data implied that BMI1 modulated miR-191 expression and mediated the osteo-inductive function of TGF-β1.

Then we examined whether and how BMI1 affected miR-191 transcription. Results from the ChIP assay demonstrated that overexpression of BMI1 fully blocked the binding of SMAD2 at all binding sites of the miR-191 promoter (Figure 6E). Luciferase assay confirmed that *Bmi1* overexpression significantly reduced the promotive effect of SMAD2 on the reporter activity of miR-191 while slightly increased the reporter activity of miR-191 5′UTR in a dose-independent manner per se (Figure 6F). PCR results confirmed that *Bmi1* overexpression significantly blocked the increase of miR-191 induced by *Smad2* overexpression (Figure 6G). Collectively, the above data confirmed that BMI1 disrupted the activation of miR-191 by SMAD2.

Next, we explored the mechanism by which BMI1 impeded SMAD2 binding to the miR-191 promoter. As shown in Figure 6H, one binding site for BMI1 (−986 to −1,008 bp from the transcription start site at miR-191) was found at the promoter of miR-191, the site lying between the S4 and S5 binding sites for SMAD2, as predicted by animal TFDB (https://guolab.wchscu.cn/AnimalTFDB4/#/) (Figure 6H). The ChIP-PCR assay verified significant binding of BMI1 at the miR-191 promoter when BMI1 was overexpressed; the elevation of SMAD2 significantly facilitated BMI1 binding at the miR-191 promoter as well (Figure 6I), suggesting that SMAD2 recruited BMI1 to the miR-191 promoter. Co-delivery of SMAD2 and BMI1 significantly enhanced the binding of BMI1 (Figure 6I), but diminished the binding of SMAD2 at the miR-191 promoter (Figure 6F), all of which indicated that BMI1 might compete with SMAD2 for binding to the miR-191 promoter. Further competitive DNA pull-down assays confirmed that both SMAD2 and BMI1 could bind to the biotin-labeled miR-191 promoter; as the amount of BMI1 in the

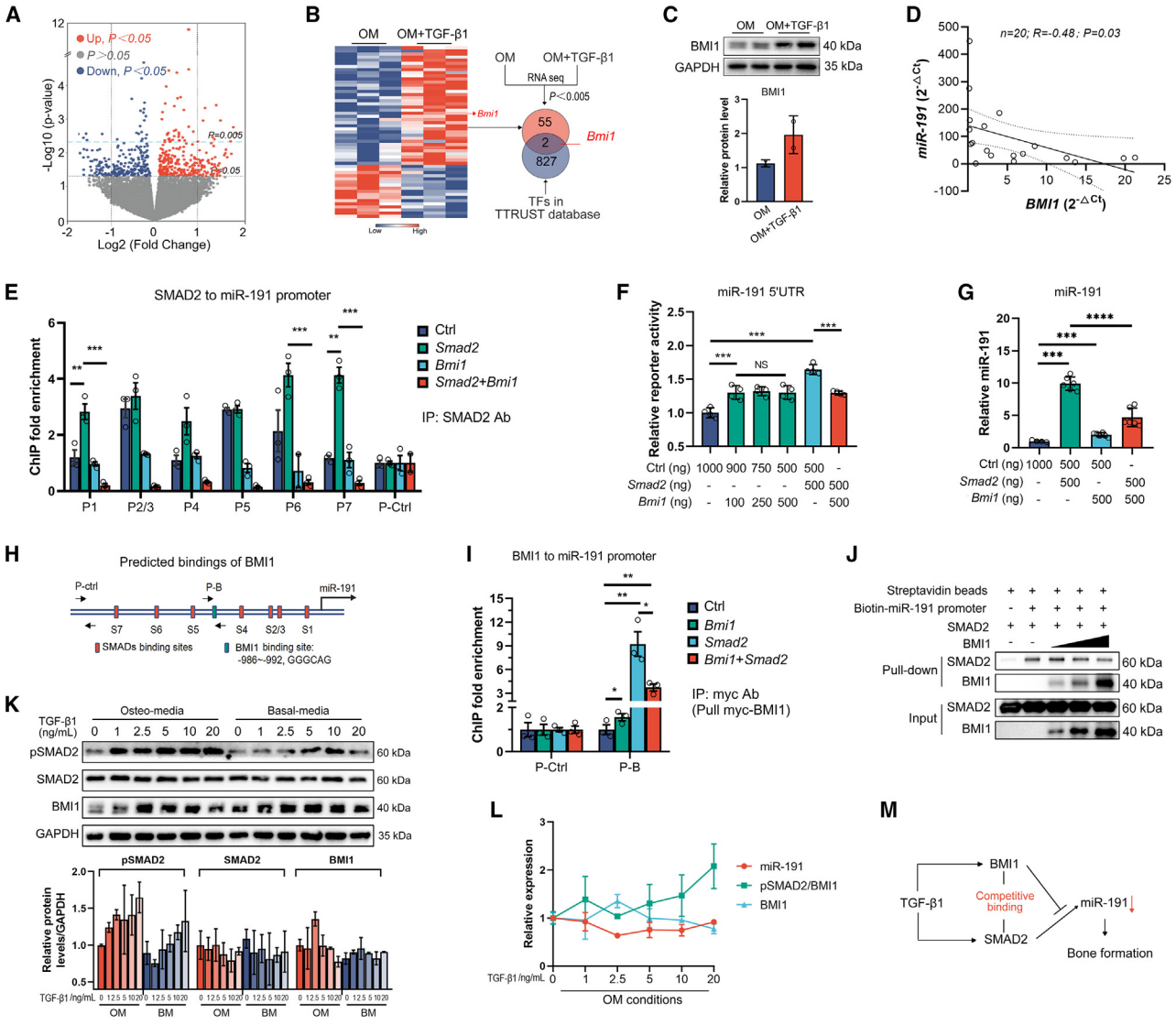

Figure 6. TGF-β1-triggered BMI1 regulates the expression of miR-191 via interacting with SMAD2

(A) Volcano plots of deregulated genes in murine BMSCs cultured in OM and OM with TGF-β1 (2.5 ng/mL). (B) Common genes between the deregulated genes in OM/OM with TGF-β1-treated BMSCs and murine transcription factors in the TRRUST database. (C) Protein levels of BMI1 in BMSCs cultured in the indicated media. (D) The correlation analysis of *BMI1* with miR-191 in human bone tissues. (E) ChIP assays of SMAD2 on the miR-191 promoter in HEK293T cells transfected with pHAGE-Ctrl (Ctrl)/pHAGE-*Bmi1* (*Bmi1*)/pHAGE-*Smad2* (*Smad2*)/pHAGE-*Bmi1* and pHAGE-*Smad2* (*Bmi1*+*Smad2*) (10 μg) in 10 cm dishes. The data are presented as the mean ± SEMs. (F) Luciferase analysis of reporter activity of miR-191 5′UTR in HEK293T cells after transfecting with the indicated plasmids. The data are presented as the mean ± SDs. (G) miR-191 levels in HEK293T cells following transfection using the indicated plasmids in 12-well plates. The data are presented as the mean ± SDs. (H) The predicted sequence of the BMI1 binding site at the miR-191 promoter. "P-B" represents the primer position for the binding site of BMI1. (I) ChIP assays of BMI1 on the miR-191 promoter in HEK293T cells transfected with the indicated plasmids (10 μg) in 10-cm dishes. The data are presented as the mean ± SEMs. (J) For the competitive DNA pull-down assay, purified flag-tagged SMAD2 was mixed with the biotinylated miR-191 promoter, and then purified BMI1 proteins were added at different dosages. The precipitates of Dynabeads Streptavidin were analyzed by western blotting with BMI1 and SMAD2 antibodies. The data are presented as the mean ± SEMs. (K) Western blotting analysis of protein levels of pSMAD2, total SMAD2, and BMI1 in BMSCs cultured under the indicated conditions. The data are presented as the mean ± SEMs. (L) The levels of miR-191, BMI1, and pSMAD2/BMI1 in BMSCs in response to varying concentrations of TGF-β1 under osteogenic conditions. (M) Schematic diagram of the regulatory mode of BMI1 and SMAD2 on the expression of miR-191 upon TGF-β1 stimulation. The significance is shown as *p < 0.05, **p < 0.01, ***p < 0.001, and ****p < 0.0001.

reaction system increased, BMI1's binding to the promoter of miR-191 gradually increased, whereas SMAD2's binding exhibited a gradual decrease (Figure 6J).

To clarify the relationship among miR-191, BMI1, and SMAD2, we assessed the expression of BMI1 and pSMAD2 at different concentrations of TGF-β1. The results showed that the overall pSMAD2 levels

were higher in BMSCs cultured in OM compared with basal media, and the expression of BMI1 was enhanced by 2.5 ng/mL TGF-β1. However, a high level of TGF-β1 (20 ng/mL) resulted in increased SMAD2 activation, but concurrently, BMI1 expression was reduced (Figure 6K), suggesting that the level changes of BMI1 and pSMAD2 might be closely related to the expression of miR-191. Therefore, we analyzed the ratio of pSMAD2 to BMI1 expression levels at different concentrations of TGF-β1 under osteogenic conditions. As Figure 6L shows, the changes in the ratio of pSMAD2 to BMI1 expression levels were largely consistent with the changes in miR-191 levels (a decrease at 2.5 ng/mL and a recovery at 10 or 20 ng/mL), while the expression trend of BMI1 was opposite to that of miR-191. The above findings further confirmed that miR-191 expression was strictly regulated by both BMI1 and pSMAD2 in response to TGF-β1 under osteogenic conditions. Therefore, we concluded that TGF-β1 upregulated BMI1, which bound to the miR-191 promoter and competitively disrupted SMAD2 binding to the miR-191 promoter and inhibited the transcriptional activation of miR-191 by SMAD2, thus maintaining a lower level of miR-191 in BMSCs (Figure 6K), and ultimately enhancing osteogenesis and bone formation.

DISCUSSION

TGF-β1 is highly activated during bone repair and is essential for bone formation and fracture healing.[45,46] Although it is considered as a bone-forming agent to promote bone healing, TGF-β1 also enhances bone resorption under certain conditions.[11] In addition, TGF-β1 participates in diverse biological processes outside the bone environment.[16,47] Thus, rather than control general TGF-β1 responses, modulating specific targets of TGF-β1 that mediate certain TGF-β1 responses is more effective for therapeutic development. Our present study demonstrated miR-191 as a key downstream target of TGF-β1 signaling under the osteogenic microenvironment. Osteo-favoring TGF-β1 downregulated miR-191. In human bone tissues, miR-191 was decreased more in children than in middle-aged individuals, implying the association of low miR-191 and active bone formation in children. MiR-191 deficiency significantly induced bone mass, mineral deposition, and bone repair by enhancing the osteogenesis, paracrine effect, and migration of BMSCs. The potential clinical translational value of miR-191 was also verified by a hydrogel-based bone repair model, implying miR-191 as a promising therapeutic target for bone repair.

SMAD2 and SMAD3 serve as key mediators of TGF-β signaling, but their selective transcriptional responses in transducing TGF-β were largely unknown.[48] We identified miR-191 as a specific target of SMAD2. Although oligomerization with SMAD4 was necessary for SMAD2 to activate TGF-β-mediated transcription of target genes,[49] we observed that SMAD4 overexpression alone was not sufficient to activate miR-191, implying the important function of nuclear translocation of SMAD2/SMAD4 complex in miR-191 activation. We also found an inhibition of BMI1 on TGF-β1/SMAD2-mediated activation of miR-191, whether BMI1 selectively regulates SMAD2-, but not SMAD3- or SMAD4-mediated transcriptional responses will be explored in our future study.

In our study, BMI1 was significantly increased upon osteo-favoring TGF-β1 stimuli under osteogenic conditions and the influence of TGF-β1 is partially dependent on BMI1. BMI1 is an essential epigenetic repressor of target genes via the PRC1 complex; however, we observed that BMI1 activated the expression of osteo-favoring markers of *Col1a1*, *Ocn*, and *Osx*, which were initiated by TGF-β1, whereas it suppressed the expression of miR-191, which was inhibited by TGF-β1, implying a dual function of BMI1 in the regulation of osteogenesis-related genes. Indeed, BMI1 has been reported to have both a transcriptionally activating role and a transcriptionally repressing role in gene regulation,[50,51] but the evidence about the bidirectional regulation of BMI1 on the target genes involved in a certain biological process, such as osteogenesis in our study, was very limited. In addition, PCGF5 has been reported to repress the SMAD2/TGF-β signaling pathway,[23] but BMI1 mediated TGF-β1 signaling in our study, indicating the context-specific function of PRC1 subunits in the regulation of the same signaling pathway. Furthermore, whether BMI1 controls the expression of miR-191 or other SMAD2 downstream targets in a PRC1-dependent manner through modulating H2AK119ub1 and H3K4me3 of target promoter will be deciphered in future studies.

We revealed a novel BMI1-SMAD2 competitive pattern regulating miR-191 transcription, which was achieved by BMI1 occupying its binding site to dissociate SMAD2 from the adjacent binding sites on the miR-191 promoter. Recently, a similar regulatory mode of other transcription factors has been reported, in which the transcription factor p53 competes with EZH2 for the same binding region in the Neat1 promoter, and blocks the transcriptional activation of EZH2 to the Neat1 gene.[52] Together with our findings, these results implied that shifting the binding of transcription factors to specific genes was an important way in which cells rapidly regulated select genes in response to diverse microenvironmental cues. Notably, a previous report demonstrated that BMI1, SMAD2, and RUNX2 could bind to the promoters of the same genes modulating the fate commitment of embryonic stem cells by using sequential ChIP-PCR.[53] Our study demonstrated miR-191 as a common target of BMI1 and SMAD2, but whether BMI1, SMAD2, and RUNX2 could form a complex and function in bone formation will be investigated in our future study. Above all, our work further enriched the interplay paradigm of transcription factors mediating certain TGF-β1 responses.

Moreover, transcription factors, including BMI1 and SMADs, are all widely expressed in various tissues, and they regulate diverse genes depending on specific signals,[47,54–56] which limits their use as therapeutic targets in the clinic. As a common target of BMI1 and SMAD2, miR-191 effectively modulated the function of BMSCs and overcame the limit of BMI1 and SMAD2 as drug targets, displaying great potential in bone regeneration. In the future, the relationship between miR-191 and aging or aging-related bone diseases such as osteoporosis will be investigated. The effect of miR-191 inhibition on larger bone defects, such as rat cranial defects needs further analysis.

In conclusion, we demonstrated that miR-191, downregulated by an osteo-favoring TGF-β1 under osteogenic conditions, plays an

essential role in bone formation. MiR-191 deficiency enhanced bone formation and repair via regulating the osteogenesis of BMSCs. MiR-191 was transcriptionally controlled by a novel interplay of transcription factors BMI1 and SMAD2, in which BMI1 competed with SMAD2 for binding to miR-191 promoter, subsequently disturbing the activation of SMAD2 on miR-191. Our findings revealed a novel regulation mechanism between miR-191 and BMI1/SMAD2, and demonstrated inhibition of miR-191 may be a promising strategy to promote bone formation.

MATERIALS AND METHODS

Animals and approvals

All procedures of animal experiments in our present study adhered to the Guide for the Care and Use of Laboratory Animals (NIH publication no. 80–23, revised 1996). The experiments were also approved by the Animal Care and Use Committee of Wuhan Union Hospital. C57BL/6 mice were purchased from the Animal Experiment Center of Huazhong University of Science and Technology or Vital River Laboratory Animal Technology (Beijing, China). MiR-191 gene (chromosome 9: 108445518–108445591) was globally deleted in mice, as we described in our earlier report.[25] All mice were in a controllable environment with 12 h of light and dark cycle, stable humidity and temperature, and freely accessible food and water.

Human specimens

The Ethics Committee of the Union Hospital of Tongji Medical College approved our project (Ethics no. 2020-S001). All experiments followed the guidelines. Human bone specimens were acquired from orthopedic surgery patients at Wuhan Union Hospital. These bone tissues would typically be discarded after surgeries. Thirty-seven patients were included in the study, with 18 samples between the ages of 40 and 55 and 19 samples in the 1–14 age range. The basal information of these patients is shown in Table S2. Subjects receiving treatment with steroids, hormones, bisphosphonate, or calcitonin, which might influence bone metabolism, were excluded.

Re-analysis of GSE datasets

Our study aimed to identify microRNAs that are regulated by TGF-β1 under osteogenic condition. We did not find GSE data that fully met the requirements. Therefore, we obtained sequencing data of differentially expressed microRNAs during the osteogenesis of BMSCs at days 0, 1, 3, 7, 10, and 13 from the GEO database (GEO: GSE107297). We selected 87 differentially expressed microRNAs with basemean ≥ 500 (basemean refers to the average gene expression level in the day 0 group). Then, we re-analyzed the sequencing data of differentially expressed microRNAs in response to the activation or inactivation of TGF-β1 signaling (GEO: GSE39994, TGF-β1 activator: doxycycline treatment, TGF-β1 inhibitor: SB-431541 treatment, mouse embryonic stem cells). Considering the opposite effects of TGF-β1 activation and inhibition on the same molecules, we conducted a screening analysis. We identified 101 microRNAs that were downregulated upon TGF-β1 activation and upregulated following TGF-β1 inactivation, as well as 234 microRNAs that were upregulated upon TGF-β1 activation and downregulated following TGF-β1 inhibition. From these 334 genes, we chose 17 differentially expressed microRNAs with a basemean ≥ 500 and $|\log FC| \geq 0.25$ as candidates regulated by TGF-β1 signaling. Finally, we identified five common microRNAs, including miR-423-5p, miR-191-5p, miR-130a-3p, miR-199b-3p, and miR-199a-3p, among 87 microRNAs regulated by osteogenesis and 17 microRNAs modulated by TGF-β1 signaling. The expression of the five microRNAs was validated by qPCR, and miR-191 was selected for further study.

Harvesting of BMSCs

Bone marrow stromal cells were harvested by flushing bone marrow from the hind limbs of 4- to 6-week-old mice, followed by culturing in IMDM (HyClone) supplemented with 10% FBS. The media were changed twice over 14 days, and adherent cells were passaged and cultured in complete IMDM. Flow cytometry was employed to verify the purity of BMSCs by using surface staining with positive markers including CD105, CD73, and CD90, and negative markers including CD45 and CD34. BMSCs from passages 2–5 were utilized for differentiation, migration, and transfection assays.

Osteoblastic differentiation

BMSCs were plated in 12-well plates (5,000 cells/cm^2). Osteogenesis was induced by the OM, which is complete IMDM supplemented with dexamethasone (0.1 nM), β-glycerophosphate (10 mM), and ascorbic acid (50 μM). We changed culture media every 3 days. The calcium deposition was evaluated through Alizarin Red staining. The levels of ALP were measured by using ALP activity detection kit (Nanjing Jiancheng, A059-2-2) according to the manufacturer's instructions.

Transwell migration assay

Cell migration was assessed using Transwell inserts with 8.0 μM pore size (Corning, 24-well format). BMSCs (1×10^5/insert) were cultured in complete media in the top compartment. Meanwhile, the lower compartment was filled with complete media with TGF-β1 (2.5 ng/mL, Pepro Tech). After incubation for 16 h, the cells on the top side of the insert membrane were wiped away, and those that migrated to the lower side of the membrane were treated utilizing paraformaldehyde (PFA) and stained using crystal violet (Sigma, C3886). Cells were photographed with microscopy (MSHOT, China) and analyzed by using ImageJ.

GelMA hydrogel preparation

GelMA hydrogel was prepared as we previously reported.[57] For GelMA synthesis, 1 g porcine skin gelatin was dissolved in 10 mL PBS, then 0.6 mL of methacrylic anhydride was added and stirred at 50°C for 4 h for gelatin methacrylation. Then ice-cold acetone was added, and the subsequent precipitates were purified by using 8–14 kDa molecular weight cutoff dialysis tubing. The dialyzed GelMA was lyophilized for 72 h and stored at −20°C before use. The methacrylation ratio was above 70% following this protocol determined using 1H-NMR (Bruker 500 MHz instrument). For GelMA hydrogel-based tissue culture, BMSCs (the total number of cells in each sample was 2.5×10^5) were photo-encapsulated in

10% w/v GelMA hydrogels (the size of each hydrogel is 5 mm in diameter/2.5 mm in thickness) and cultured in complete media IMDM or OM. The culture media was changed every 3 days. For cell viability assay, hydrogels embedded with BMSCs were stained using the live/dead viability kit (#L3224, Thermo) and then sliced into thin sections for observation under a microscopy.

Tibia monocortical defect model

The tibial monocortical defect model was constructed as previously described.[58,59] Skeletally mature male mice aged 9–12 weeks were used for all studies. Through intraperitoneal injection with sodium pentobarbital (100 mg/kg), the animals were anesthetized, and then after a careful incision over the medial side of diaphysis, the tibia muscle was dissected, exposing the medial side of tibia. A Dremel drill bit was used to create a hole (0.8 mm in diameter) penetrating one cortex. A hole (0.8-mm diameter) penetrating one cortex was created using a drill bit (Dremel). The site was washed with saline to eliminate bone fragments. Then the incision was sealed using nonabsorbable sutures. To alleviate pain, all mice were subcutaneously injected with 0.05–0.1 mg/kg buprenorphine after surgery. For hydrogel-based therapy, miR-191 inhibitor-transfected BMSCs were mixed with GelMA solutions (15% w/v) in water bath at 37°C, and then the mixture was added to the defect sites (5 μL/defect) with micropoint pipette tips. Immediately after addition, the defect was exposed to longwave UV light (395 nm, UVA) for 10 min to ensure gel patterning. During all procedures, bleeding was controlled by compression with aseptic cotton.

μCt

The femurs or tibias were acquired and treated with 4% PFA to fix overnight, and then in 70% ethanol until use. A μCT system (SkyScan1176, Bruker) was used to scan the skulls, the spatial resolution being 9 μm. Three-dimensional histomorphometric analysis was carried out using sagittal image sections of specimens as reported.[42] Trabecular and cortical bone parameters were quantified using NRecon image reconstruction software, CTAn-analysis software, and CTvol-3D model visualization software. In the distal femur, the range of region of interest selected for analysis started from 50 pieces below growth plate to 400 pieces up straight. The parameters including bone volume per tissue volume (Tb.BV/TV), trabecular number (Tb.N), trabecular separation (Tb.Sp), and trabecular thickness (Tb.Th) were examined. For cortical bone, cortical thickness (Ct.Th) was analyzed; 3D reconstruction was conducted using cross-sectional images.

Histological analysis

The skull samples were fixed with 4% PFA and immersed in 0.5 M EDTA (pH 8.0) for at least 14 days to be decalcified. Then embedded samples were longitudinally sliced into 5-μm thickness. For immunostaining, sections were exposed to primary antibodies against collagen 1 (1:100; ABclonal, A16891) overnight at 4°C. Following this, sections were immersed in secondary antibodies and incubated at 37°C for 30 min. Hematoxylin counterstaining was then performed.

ChIP assay

A ChIP assay was used to analyze the binding of BMI1 and SMAD2 to the miR-191 promoter. The ChIP assay kit was purchased from CST, and the manufacturer's instructions were followed. Briefly, HEK293T cells were fixed with 1% formaldehyde, sonicated, and immunoprecipitated with anti-SMAD2 antibody (1:50, CST, #5339), anti-Myc antibody (1:50, CST, #2276), and normal rabbit immunoglobulin G (1:50, CST, #3900) together with protein G magnetic beads (CST, #9006). The precipitates were thoroughly washed. Then the DNA was purified using a DNA fragment purification kit (Solarbio, Beijing, T0250) and analyzed by PCR using specific primers. PCR was conducted to analyze the purified DNA, and PCR primers and the PCR product informations including their length and loci on the genome are shown in Table S5.

Plasmids

Oligos including mimics of mus-miR-191-5p, inhibitors of mus-miR-191-5p, and corresponding controls were provided by Ribo Biotechnology (Guangzhou, China). Mouse cDNA of *Smad2*, *Smad3*, *Smad4*, and *Bmi1* were amplified, and ligated into the pHAGE-Flag or pHAGE-Myc vector. MiR-191 promoter (chromosome 9: 108443518–108445518) was amplified and ligated into the pGL3-basic vector. The target sequence accuracy of all plasmids was confirmed through sequencing. The over- and down-regulation of genes was detected by RT-PCR and western blotting.

Luciferase reporter assay

HEK293T cells were co-transfected with pGL3-miR-191-5′UTR, pRL-TK, and pHAGE-*Smad2*, *Smad3*, *Smad4*, or *Bmi1* for 48 h. To assess the reporter activities, cells were lysed and underwent a dual luciferase assay from Promega (Madison, WI).

Cytometric bead array

Cytokines including interleukin (IL)-10, IL-6, IL-12p70, monocyte chemoattractant protein-1 (MCP-1), and interferon gamma (IFN-γ) were evaluated using a Mouse Inflammation CBA Kit (BD Biosciences). The supernatant of BMSCs following transfection with oligos and treated with OM for 48 h was analyzed by flow cytometry. The data were visualized by FCAP Array software and FlowJo software.

DNA pull-down assay

Biotinylated miR-191 promoter single-strand DNA (ssDNA) was prepared using Biotin DNA Labeling Mix (Pierce, #89818). Flag-tagged BMI1 and Flag-tagged SMAD2 were purified based on a 293-F eukaryotic expression and purification system. The purified protein was verified by Coomassie Blue staining and western blotting. For the pull-down assay, biotinylated miR-191 promoter ssDNAs were incubated with purified SMAD2 (10 μg), BMI1 (0, 2.5, 5, and 10 μg), and Dynabeads M280 streptavidin (25 μL per sample, Invitrogen, #11205D). To reduce nonspecific protein binding of beads, equal amounts of 5% BSA (w/v) were added into the bead solution. After incubation, the precipitates were washed at least five times using a washing buffer containing 5 mM Tris-HCl, pH 7.5, 1 M NaCl, and

0.5 mM EDTA. The remaining proteins were detected by western blotting.

Quantitative PCR and western blotting

Total RNA was isolated from the specimens; 1 μg of the RNA was reversely transcribed and the generated cDNA was quantified using RT-PCR via a Quantagene q225 System (Kubotechnology, China). The reagents for microRNA detection were purchased from Ribo Biotechnology (Guangzhou, China). U6 snRNA or GAPDH were included as the reference genes for normalization. Table S6 shows the PCR primers. Western blotting was performed following a previous protocol.[60] The antibodies utilized in this study included the following: anti-collagen 1 antibody (ABclonal, A16891), anti-SMAD2 antibody (CST, #5339), anti-BMI1 antibody (CST, #5856), and anti-pSMAD2 antibody (CST, #3108). Signals were detected using enhanced chemiluminescence (Bio-Rad).

Double calcein labeling

Male mice aged 6 weeks were intraperitoneally injected with calcein (20 mg/kg, Sigma, #C0875) at 6 and 2 days before they were euthanized. Femurs were fixed in 4% PFA, embedded, and sectioned into 10 μm slices with a Leica microtome. Calcein labeling was visualized using a microscope and CaseViewer. The distance between the double-labeled bands of cortical bones was measured using ImageJ. As previously reported,[61] the midpoint distance was calculated from six double labels per sample, and then we divided that length by the number of days between calcein injections (4 days in our study). The bone formation rate per bone perimeter (BFR/B.Pm, $\mu m^2/\mu m/d$) was computed using the formula: BFR/B.Pm = MAR×(dL.Pm+sL.Pm/2)/B.Pm, where dL.Pm represented the length of the double labels, and sL.Pm represented the length of the single labels.

Enzyme-linked immunosorbent assay

The serum content of CTX-I and P1NP were measured using ELISA kits from Elabscience (P1NP, #E-EL-M0233c; CTX-I, #E-EL-M3023, Wuhan, China). Serum samples were diluted 10- and 2-fold prior to ELISA for P1NP and CTX-I, respectively.

RNA sequencing and data analysis

BMSCs were treated with OM or OM supplemented with TGF-β1 (2.5 ng/mL, OM+TGF-β1). After 48 h incubation, total RNA was isolated for RNA sequencing. The resulting raw reads were assessed with FastQC. Trim_galore (version 0.4.4) was employed to remove the low-quality bases and adaptor sequences from our sequencing reads. DEGs ($p \leq 0.005$, $|\log_2 \text{fold change}|$ greater than 0.3) were compared with all transcription factors provided by the TRRUST database (https://www.grnpedia.org/trrust/downloadnetwork.php) to obtain common genes for further study. To identify genes regulated by miR-191, BMSCs were transfected with I-ctrl or I-miR-191 for 24 h, and cultured in osteogenic induction media for 48 h. After RNA sequencing, all DEGs ($p < 0.05$) were subjected to DAVID analysis (https://david.ncifcrf.gov/). A heatmap was modeled by the online Morpheus (https://software.broadinstitute.org/morpheus/). The raw data has been uploaded in GSA:PRJCA024333.

Statistical analysis

All statistical analyses were done using Excel or GraphPad Prism8. An unpaired Student's t test was used to assess statistical significance. When a p value was less than 0.05, we regarded it as statistically significant. Data are presented as mean ± SD.

DATA AND CODE AVAILABILITY

The data related to this study are fully documented in the paper or the supplemental information.

SUPPLEMENTAL INFORMATION

Supplemental information can be found online at https://doi.org/10.1016/j.omtn.2024.102164.

ACKNOWLEDGMENTS

We thank Dr. Guangshuo Ou for providing help in RNA sequencing and corresponding data analysis, Dr. Xiaodong Zhang for providing several experimental materials, Dr. Ying Liu for providing technical assistance with the flow cytometry, and Dr. Hongjun Yu for offering assistance in protein purification. We also thank Dr. Guangshuo Ou and Dr. Xiaodong Zhang for helpful discussion. This research study was supported by the National Natural Science Foundation of China, nos. 82370647 (W.H.), 82170642 (J.-X.Z.), 81801923 (X.-F.Z.), 81670575 (J.-X.Z.), 81570570 (W.H.) and 81070355 (J.-X.Z.), the Program of HUST Academic Frontier Youth Team, Huazhong University of Science and Technology (2018QYTD02), and the Pre-Research Fund for Free Innovation of Union Hospital, Huazhong University of Science and Technology (nos. 02.03.2017-312 and 02.03.2018-126).

AUTHOR CONTRIBUTIONS

H.W., J.-X.Z., and X.-F.Z. conceived and supervised the work. X.-F.Z., Z.-X.W., B.-W.Z., and T.-X.R. performed *in vitro* and *in vivo* experiments. K.-P.H., X.C., T.W., and P.H. assisted the isolation of primary MSCs, and the construction of plasmids. J.L., W.-H.X., X.-F.Z., Z.-X.W., and X.C. collaborated to collect human specimens. X.-F.Z. and Z.-X.W. visualized the data. H.W., J.-X.Z., and X.-F.Z. acquired funds. X.-F.Z., H.W., and Z.-X.W. drafted the manuscript.

DECLARATION OF INTERESTS

The authors declare no competing interests.

REFERENCES

1. Salhotra, A., Shah, H.N., Levi, B., and Longaker, M.T. (2020). Mechanisms of bone development and repair. Nat. Rev. Mol. Cell Biol. *21*, 696–711.

2. Long, F. (2011). Building strong bones: molecular regulation of the osteoblast lineage. Nat. Rev. Mol. Cell Biol. *13*, 27–38.

3. Sivaraj, K.K., Majev, P.G., Jeong, H.W., Dharmalingam, B., Zeuschner, D., Schröder, S., Bixel, M.G., Timmen, M., Stange, R., and Adams, R.H. (2022). Mesenchymal stromal cell-derived septoclasts resorb cartilage during developmental ossification and fracture healing. Nat. Commun. *13*, 571.

4. Lin, H., Sohn, J., Shen, H., Langhans, M.T., and Tuan, R.S. (2019). Bone marrow mesenchymal stem cells: Aging and tissue engineering applications to enhance bone healing. Biomaterials *203*, 96–110.

5. Hasani-Sadrabadi, M.M., Sarrion, P., Pouraghaei, S., Chau, Y., Ansari, S., Li, S., Aghaloo, T., and Moshaverinia, A. (2020). An engineered cell-laden adhesive hydrogel promotes craniofacial bone tissue regeneration in rats. Sci. Transl. Med. *12*, eaay6853.
6. Grayson, W.L., Bunnell, B.A., Martin, E., Frazier, T., Hung, B.P., and Gimble, J.M. (2015). Stromal cells and stem cells in clinical bone regeneration. Nat. Rev. Endocrinol. *11*, 140–150.
7. Majidinia, M., Sadeghpour, A., and Yousefi, B. (2018). The roles of signaling pathways in bone repair and regeneration. J. Cell. Physiol. *233*, 2937–2948.
8. Janssens, K., ten Dijke, P., Janssens, S., and Van Hul, W. (2005). Transforming growth factor-beta1 to the bone. Endocr. Rev. *26*, 743–774.
9. Dole, N.S., Mazur, C.M., Acevedo, C., Lopez, J.P., Monteiro, D.A., Fowler, T.W., Gludovatz, B., Walsh, F., Regan, J.N., Messina, S., et al. (2017). Osteocyte-Intrinsic TGF-β Signaling Regulates Bone Quality through Perilacunar/Canalicular Remodeling. Cell Rep. *21*, 2585–2596.
10. Xu, J., Liu, J., Gan, Y., Dai, K., Zhao, J., Huang, M., Huang, Y., Zhuang, Y., and Zhang, X. (2020). High-Dose TGF-β1 Impairs Mesenchymal Stem Cell-Mediated Bone Regeneration via Bmp2 Inhibition. J. Bone Miner. Res. *35*, 167–180.
11. Tang, Y., Wu, X., Lei, W., Pang, L., Wan, C., Shi, Z., Zhao, L., Nagy, T.R., Peng, X., Hu, J., et al. (2009). TGF-beta1-induced migration of bone mesenchymal stem cells couples bone resorption with formation. Nat. Med. *15*, 757–765.
12. Derynck, R., and Zhang, Y.E. (2003). Smad-dependent and Smad-independent pathways in TGF-beta family signalling. Nature *425*, 577–584.
13. Alliston, T., Choy, L., Ducy, P., Karsenty, G., and Derynck, R. (2001). TGF-beta-induced repression of CBFA1 by Smad3 decreases cbfa1 and osteocalcin expression and inhibits osteoblast differentiation. Embo j *20*, 2254–2272.
14. Crane, J.L., and Cao, X. (2014). Bone marrow mesenchymal stem cells and TGF-β signaling in bone remodeling. J. Clin. Invest. *124*, 466–472.
15. Hata, A., and Chen, Y.G. (2016). TGF-β Signaling from Receptors to Smads. Cold Spring Harb. Perspect. Biol. *8*, a022061.
16. Budi, E.H., Duan, D., and Derynck, R. (2017). Transforming Growth Factor-β Receptors and Smads: Regulatory Complexity and Functional Versatility. Trends Cell Biol. *27*, 658–672.
17. Aranda, S., Mas, G., and Di Croce, L. (2015). Regulation of gene transcription by Polycomb proteins. Sci. Adv. *1*, e1500737.
18. Li, J., Wang, Q., Yang, R., Zhang, J., Li, X., Zhou, X., and Miao, D. (2017). BMI-1 Mediates Estrogen-Deficiency-Induced Bone Loss by Inhibiting Reactive Oxygen Species Accumulation and T Cell Activation. J. Bone Miner. Res. *32*, 962–973.
19. Sun, W., Qiao, W., Zhou, B., Hu, Z., Yan, Q., Wu, J., Wang, R., Zhang, Q., and Miao, D. (2018). Overexpression of Sirt1 in mesenchymal stem cells protects against bone loss in mice by FOXO3a deacetylation and oxidative stress inhibition. Metabolism *88*, 61–71.
20. Zheng, X., Wang, Q., Xie, Z., and Li, J. (2021). The elevated level of IL-1α in the bone marrow of aged mice leads to MSC senescence partly by down-regulating Bmi-1. Exp. Gerontol. *148*, 111313.
21. Zhang, H.W., Ding, J., Jin, J.L., Guo, J., Liu, J.N., Karaplis, A., Goltzman, D., and Miao, D. (2010). Defects in mesenchymal stem cell self-renewal and cell fate determination lead to an osteopenic phenotype in Bmi-1 null mice. J. Bone Miner. Res. *25*, 640–652.
22. Liu, J., Cao, L., Chen, J., Song, S., Lee, I.H., Quijano, C., Liu, H., Keyvanfar, K., Chen, H., Cao, L.Y., et al. (2009). Bmi1 regulates mitochondrial function and the DNA damage response pathway. Nature *459*, 387–392.
23. Yao, M., Zhou, X., Zhou, J., Gong, S., Hu, G., Li, J., Huang, K., Lai, P., Shi, G., Hutchins, A.P., et al. (2018). PCGF5 is required for neural differentiation of embryonic stem cells. Nat. Commun. *9*, 1463.
24. Nagpal, N., and Kulshreshtha, R. (2014). miR-191: an emerging player in disease biology. Front. Genet. *5*, 99.
25. Pan, W., Wang, L., Zhang, X.F., Zhang, H., Zhang, J., Wang, G., Xu, P., Zhang, Y., Hu, P., Zhang, X.D., et al. (2019). Hypoxia-induced microRNA-191 contributes to hepatic ischemia/reperfusion injury through the ZONAB/Cyclin D1 axis. Cell Death Differ. *26*, 291–305.
26. Chaudhry, M.A., Omaruddin, R.A., Brumbaugh, C.D., Tariq, M.A., and Pourmand, N. (2013). Identification of radiation-induced microRNA transcriptome by next-generation massively parallel sequencing. J. Radiat. Res. *54*, 808–822.
27. Xu, X., Zhou, X., Zhang, J., Li, H., Cao, Y., Tan, X., Zhu, X., and Yang, J. (2020). MicroRNA-191 modulates cisplatin-induced DNA damage response by targeting RCC2. Faseb j *34*, 13573–13585.
28. Acuña-González, R.J., Olvera-Valencia, M., López-Canales, J.S., Lozano-Cuenca, J., Osorio-Caballero, M., and Flores-Herrera, H. (2021). MiR-191-5p is upregulated in culture media of implanted human embryo on day fifth of development. Reprod. Biol. Endocrinol. *19*, 109.
29. Hadjimichael, C., Nikolaou, C., Papamatheakis, J., and Kretsovali, A. (2016). MicroRNAs for Fine-Tuning of Mouse Embryonic Stem Cell Fate Decision through Regulation of TGF-β Signaling. Stem Cell Rep. *6*, 292–301.
30. Chang, C.C., Venø, M.T., Chen, L., Ditzel, N., Le, D.Q.S., Dillschneider, P., Kassem, M., and Kjems, J. (2018). Global MicroRNA Profiling in Human Bone Marrow Skeletal-Stromal or Mesenchymal-Stem Cells Identified Candidates for Bone Regeneration. Mol. Ther. *26*, 593–605.
31. Zhen, G., Wen, C., Jia, X., Li, Y., Crane, J.L., Mears, S.C., Askin, F.B., Frassica, F.J., Chang, W., Yao, J., et al. (2013). Inhibition of TGF-β signaling in mesenchymal stem cells of subchondral bone attenuates osteoarthritis. Nat. Med. *19*, 704–712.
32. Lind, M., Overgaard, S., Søballe, K., Nguyen, T., Ongpipattanakul, B., and Bünger, C. (1996). Transforming growth factor-beta 1 enhances bone healing to unloaded tricalcium phosphate coated implants: an experimental study in dogs. J. Orthop. Res. *14*, 343–350.
33. Nielsen, H.M., Andreassen, T.T., Ledet, T., and Oxlund, H. (1994). Local injection of TGF-beta increases the strength of tibial fractures in the rat. Acta Orthop. Scand. *65*, 37–41.
34. Marcelli, C., Yates, A.J., and Mundy, G.R. (1990). In vivo effects of human recombinant transforming growth factor beta on bone turnover in normal mice. J. Bone Miner. Res. *5*, 1087–1096.
35. Mackie, E.J., and Trechsel, U. (1990). Stimulation of bone formation in vivo by transforming growth factor-beta: remodeling of woven bone and lack of inhibition by indomethacin. Bone *11*, 295–300.
36. Redshaw, N., Camps, C., Sharma, V., Motallebipour, M., Guzman-Ayala, M., Oikonomopoulos, S., Thymiakou, E., Ragoussis, J., and Episkopou, V. (2013). TGF-β/Smad2/3 signaling directly regulates several miRNAs in mouse ES cells and early embryos. PLoS One *8*, e55186.
37. Kurundkar, A.R., Kurundkar, D., Rangarajan, S., Locy, M.L., Zhou, Y., Liu, R.M., Zmijewski, J., and Thannickal, V.J. (2016). The matricellular protein CCN1 enhances TGF-β1/SMAD3-dependent profibrotic signaling in fibroblasts and contributes to fibrogenic responses to lung injury. Faseb j *30*, 2135–2150.
38. Bai, L., Han, X., Kee, H.J., He, X., Kim, S.H., Jeon, M.J., Zhou, H., Jeong, S.M., Kee, S.J., and Jeong, M.H. (2023). Protocatechuic acid prevents isoproterenol-induced heart failure in mice by downregulating kynurenine-3-monooxygenase. J. Cell Mol. Med. *27*, 2290–2307.
39. Polvani, G., Pompilio, G., and Sommariva, E. (2021). Excess TGF-β1 Drives Cardiac Mesenchymal Stromal Cells to a Pro-Fibrotic Commitment in Arrhythmogenic Cardiomyopathy. Int. J. Mol. Sci. *22*, 2673.
40. Pan, X., Chen, Z., Huang, R., Yao, Y., and Ma, G. (2013). Transforming growth factor β1 induces the expression of collagen type I by DNA methylation in cardiac fibroblasts. PLoS One *8*, e60335.
41. Wang, K., Guo, Z., Bao, Y., Pang, Y., Li, Y., He, H., and Song, D. (2020). Structure-Activity Relationship of Aloperine Derivatives as New Anti-Liver Fibrogenic Agents. Molecules *25*, 4977.
42. Hu, K., and Olsen, B.R. (2016). Osteoblast-derived VEGF regulates osteoblast differentiation and bone formation during bone repair. J. Clin. Invest. *126*, 509–526.
43. Kim, J.B., Leucht, P., Lam, K., Luppen, C., Ten Berge, D., Nusse, R., and Helms, J.A. (2007). Bone regeneration is regulated by wnt signaling. J. Bone Miner. Res. *22*, 1913–1923.
44. Chen, G., Zhang, Y., Yu, S., Sun, W., and Miao, D. (2019). Bmi1 Overexpression in Mesenchymal Stem Cells Exerts Antiaging and Antiosteoporosis Effects by Inactivating p16/p19 Signaling and Inhibiting. Stem Cell. *37*, 1200–1211.

45. Chen, G., Deng, C., and Li, Y.P. (2012). TGF-β and BMP signaling in osteoblast differentiation and bone formation. Int. J. Biol. Sci. *8*, 272–288.

46. Sarahrudi, K., Thomas, A., Mousavi, M., Kaiser, G., Köttstorfer, J., Kecht, M., Hajdu, S., and Aharinejad, S. (2011). Elevated transforming growth factor-beta 1 (TGF-β1) levels in human fracture healing. Injury *42*, 833–837.

47. Bertero, A., Brown, S., Madrigal, P., Osnato, A., Ortmann, D., Yiangou, L., Kadiwala, J., Hubner, N.C., de Los Mozos, I.R., Sadée, C., et al. (2018). The SMAD2/3 interactome reveals that TGFβ controls m(6)A mRNA methylation in pluripotency. Nature *555*, 256–259.

48. Brown, K.A., Pietenpol, J.A., and Moses, H.L. (2007). A tale of two proteins: differential roles and regulation of Smad2 and Smad3 in TGF-beta signaling. J. Cell. Biochem. *101*, 9–33.

49. Fink, S.P., Mikkola, D., Willson, J.K.V., and Markowitz, S. (2003). TGF-beta-induced nuclear localization of Smad2 and Smad3 in Smad4 null cancer cell lines. Oncogene *22*, 1317–1323.

50. Ganapathi, M., Boles, N.C., Charniga, C., Lotz, S., Campbell, M., Temple, S., and Morse, R.H. (2018). Effect of Bmi1 over-expression on gene expression in adult and embryonic murine neural stem cells. Sci. Rep. *8*, 7464.

51. Shen, H., Chen, Z., Ding, X., Qi, X., Cen, J., Wang, Y., Yao, L., and Chen, Y. (2014). BMI1 reprogrammes histone acetylation and enhances c-fos pathway via directly binding to Zmym3 in malignant myeloid progression. J. Cell Mol. Med. *18*, 1004–1017.

52. Yuan, J., Zhu, Q., Zhang, X., Wen, Z., Zhang, G., Li, N., Pei, Y., Wang, Y., Pei, S., Xu, J., et al. (2022). Ezh2 competes with p53 to license lncRNA Neat1 transcription for inflammasome activation. Cell Death Differ. *29*, 2009–2023.

53. Medeiros, R.B., Papenfuss, K.J., Hoium, B., Coley, K., Jadrich, J., Goh, S.K., Elayaperumal, A., Herrera, J.E., Resnik, E., and Ni, H.T. (2009). Novel sequential ChIP and simplified basic ChIP protocols for promoter co-occupancy and target gene identification in human embryonic stem cells. BMC Biotechnol. *9*, 59.

54. Gargiulo, G., Cesaroni, M., Serresi, M., de Vries, N., Hulsman, D., Bruggeman, S.W., Lancini, C., and van Lohuizen, M. (2013). In vivo RNAi screen for BMI1 targets identifies TGF-β/BMP-ER stress pathways as key regulators of neural- and malignant glioma-stem cell homeostasis. Cancer Cell *23*, 660–676.

55. Liu, X., Wei, W., Li, X., Shen, P., Ju, D., Wang, Z., Zhang, R., Yang, F., Chen, C., Cao, K., et al. (2017). BMI1 and MEL18 Promote Colitis-Associated Cancer in Mice via REG3B and STAT3. Gastroenterology *153*, 1607–1620.

56. Gonzalez, M.M., Bamidele, A.O., Svingen, P.A., Sagstetter, M.R., Smyrk, T.C., Gaballa, J.M., Hamdan, F.H., Kosinsky, R.L., Gibbons, H.R., Sun, Z., et al. (2021). BMI1 maintains the Treg epigenomic landscape to prevent inflammatory bowel disease. J. Clin. Invest. *131*, e140755.

57. Zhang, X., Li, J., Ye, P., Gao, G., Hubbell, K., and Cui, X. (2017). Coculture of mesenchymal stem cells and endothelial cells enhances host tissue integration and epidermis maturation through AKT activation in gelatin methacryloyl hydrogel-based skin model. Acta Biomater. *59*, 317–326.

58. Campbell, T.M., Wong, W.T., and Mackie, E.J. (2003). Establishment of a model of cortical bone repair in mice. Calcif. Tissue Int. *73*, 49–55.

59. Li, Z., and Helms, J.A. (2021). Drill Hole Models to Investigate Bone Repair. Methods Mol. Biol. *2221*, 193–204.

60. Zhang, X.F., Wang, T., Wang, Z.X., Huang, K.P., Zhang, Y.W., Wang, G.L., Zhang, H.J., Chen, Z.H., Wang, C.Y., Zhang, J.X., and Wang, H. (2021). Hypoxic ucMSC-secreted exosomal miR-125b promotes endothelial cell survival and migration during wound healing by targeting TP53INP1. Mol. Ther. Nucleic Acids *26*, 347–359.

61. Dempster, D.W., Compston, J.E., Drezner, M.K., Glorieux, F.H., Kanis, J.A., Malluche, H., Meunier, P.J., Ott, S.M., Recker, R.R., and Parfitt, A.M. (2013). Standardized nomenclature, symbols, and units for bone histomorphometry: a 2012 update of the report of the ASBMR Histomorphometry Nomenclature Committee. J. Bone Miner. Res. *28*, 2–17.